Sensors & Actuators: B. Chemical 344 (2021) 130265

Contents lists available at ScienceDirect

Sensors and Actuators: B. Chemical

journal homepage: www.elsevier.com/locate/snb

Photonic sensor systems for the identification of hydrocarbons and crude oils in static and flow conditions

Jorge Gil-Rostra [a,*], Sergio Quintero-Moreno [b,c,**], Víctor J. Rico [a], Francisco Yubero [a], Francisco J. Sanza [b,c], Rafael Casquel [b,c], Emilio Gallo-Valverde [d], María E. Jara-Galán [d], Paula Sanz-Sanz [e], Miguel Holgado [b,c], Agustín R. González-Elipe [a]

[a] Instituto de Ciencia de Materiales de Sevilla (CSIC-Univ. Sevilla), Avda. Américo Vespucio 49, 41092, Sevilla, Spain
[b] Center for Biomedical Technology (CTB), Universidad Politécnica de Madrid, Parque Científico y Tecnológico de la UPM, Campus de Montegancedo, 28223, Pozuelo de Alarcón, Madrid, Spain
[c] Department of Applied Physics and Materials Engineering, Escuela Técnica Superior de Ingenieros Industriales, Universidad Politécnica de Madrid, C/José Gutiérrez Abascal 2, 28006, Madrid, Spain
[d] MINSAIT (INDRA), Avda. de Bruselas 35, 28108, Alcobendas, Madrid, Spain
[e] REPSOL Technology Laboratory, Avda. Agustín de Betancourt s/n, 28935, Móstoles, Madrid, Spain

ARTICLE INFO

Keywords:
Refractive index sensor
Bragg microcavity
Near infrared hydrocarbons sensing
Crude oil sensing
Photonics
Optofluidics

ABSTRACT

Identification of hydrocarbons and crude oils is typically carried out with samples that, taken from natural sources or refineries, must be brought to the laboratory for their analysis with rather sophisticated instruments. Alternatively, *"in situ"* procedures have been also developed for this purpose. In this work, we propose the use of a series of several sensor systems based on photonic transducers in the form of chips for the identification and classification of crude oils and hydrocarbons through the determination of their refractive index in the visible and absorption in the near infrared regions of the electromagnetic spectrum. Two of the photonic transducers rely on modifications of a Bragg microcavity and they monitor the changes in visible light interference phenomena that occur in response to the variation of the refractive index of oils. The third one, in the form of a dielectric mirror, monitors the near infrared absorption of crude oils and hydrocarbons through the recording of a transflectance spectrum. The capacity of these transducers for crude oil identification is proved by the analysis of a series of oils and distilled fractions that have been properly identified and classified as a function of their density and partition of long hydrocarbon chains. The three photonic transducers are operated with optical fibers and can be used in static and dynamic modes, this latter under conditions that are especially well-suited for *"in-situ"* analysis of oil streams in real facilities. The proved resistance of the chips to high pressure and temperature conditions supports their suitability to withstand harsh working environments as those existing in extraction wells.

1. Introduction

Crude oils are complex mixtures that exist in liquid form in underground geologic formations and give rise to a combination of gas and liquid when brought to the surface. These heterogeneous phases are made of multiple components and compound families including hydrocarbons (saturated, aromatics, resins and asphaltenes), non-hydrocarbon molecules (H_2S, CO_2, N_2) and also a free water phase, either coming from the geological formations or from operations applied to improve oil recovery (water flooding) [1–3]. A key issue for the handling and use of crude oils is the application of robust and reliable methods for their identification and classification, a task for which a large variety of physical and chemical procedures have been utilized [4–10]. In a particular crude oil, the partition of hydrocarbons and the relative ratio among families of compounds present a large variability depending on petroleum source. This variability and the fact that natural

* Corresponding author at: Instituto de Ciencia de Materiales de Sevilla (CSIC-Univ. Sevilla), Avda. Américo Vespucio 49, 41092, Sevilla, Spain.
** Corresponding author at: Center for Biomedical Technology (CTB), Universidad Politécnica de Madrid, Parque Científico y Tecnológico de la UPM, Campus de Montegancedo, 28223, Pozuelo de Alarcón, Madrid, Spain.
E-mail addresses: jorge.gil@icmse.csic.es (J. Gil-Rostra), sa.quintero@upm.es (S. Quintero-Moreno).

https://doi.org/10.1016/j.snb.2021.130265
Received 12 February 2021; Received in revised form 26 May 2021; Accepted 7 June 2021
Available online 12 June 2021

crude oils do not appear as homogeneous phase liquid solutions, but as inhomogeneous mixtures that may include colloids, dispersed solids and even emulsified water [11–14], make crude oil identification a complex challenge generally requiring various analytical tools and procedures [8]. Most common approaches for oil analysis entail the quantitative determination of main hydrocarbon constituents by gas chromatography/flame ionization detection or gas chromatography/mass spectrometry methods. These techniques and other chemical analysis approaches [10] are not suitable for real time *"in-situ"* identification because they are expensive, complex and require time consuming procedures for the handling and preparation of analyte samples. In this context, the determination of the refractive index of crude oils and fractions with laboratory refractometers has revealed to be a useful identification approach through the correlation of this optical parameter with other properties such as density, viscosity, and others [15–17].

To circumvent these problems, several sensor devices formed by microparticles and other micro- and nano-structures relying on electrical, electrochemical or, most commonly, photonic principles of actuation [18] have been proposed for real time monitoring and/or for the determination of specific components, such as aromatic hydrocarbons, polyphenols or dissolved gases [19–21]. However, there is still a clear need for sensors that, applying simple principles of photonic detection and presenting high resistance when operated under harsh conditions, can work "*in situ*" depicting a robust, fast and reliable identification capacity of crude oils.

In recent works we have presented two types of photonic transducers that, relying on a light interference principle of actuation, are suitable for chemical detection through the determination of the refractive index of the analyzed liquids (henceforth, they will be dubbed as interferometric transducers, ITs). In this work, we use the term transducer for the optical elements that, when in contact with specific fluids and under illumination conditions, supply some signal characteristic of this fluid. These photonic sensors have been previously used for various applications including identification of biomolecules or the characterization of liquid solutions and mixtures. A first type of IT consists of an array of nanopillars lithographed on a small substrate area where each nanopillar is formed by a compact Bragg microcavity multilayer stack [22–24]. Herein, this IT system will be named pillared Bragg microcavity (*pillared-BM*). A second type of IT used in this work consists of a Bragg microcavity made of highly porous stacked layers and will be designated as porous Bragg microcavity (*porous-BM*) [25–27]. When these transducers are interrogated with white light, the reflected signal generates a characteristic resonance peak whose position varies with the refractive index of the liquid medium filling either the space among nanopillars [23,24] or the open porosity of the multilayer stack [26] existing in the *pillared-BM* or the *porous-BM*, respectively. As a result, we have found that, through the detection of changes in the refractive index of the examined liquids, they can determine glucose and other solutes dissolved in water [26,28] or the concentration of biological components dissolved in the medium. In the present work, we propose the combined use of both *pillared-BM* and *porous-BM* photonic transducers for a more reliable, rapid, and robust identification of hydrocarbons, crude oils, and their fractions and mixtures. Moreover, taking advantage of the possibility to operate these transducers with optical fibers, we report how they might be used for "*in situ*" oil monitoring.

For the analysis of crude oils, in addition to these ITs, we also propose the use of a near infrared (NIR) transducer working in transflectance geometry [29–32]. The key point that differentiates the system developed herein from other conventional NIR devices is the use of chemically resistant mirrors (dubbed here NIRM transducers) that are tailored designed to maximize their reflectance and optical performance to monitor specific wavelength regions of the NIR spectrum. We show that the ITs permit the direct determination of parameters that, related with the actual refractive index of the crude oils, can be linked with their density and other relevant properties used for oil identification [15–17]. In turn, the NIRM transducer, through the direct assessment of the absorption spectrum of the crude oils, may provide information about the particle content (e.g., asphaltenes [11–14]), C–H bonding characteristics of the constituent hydrocarbons, and the presence of water emulsions or dissolved natural gas, among others. Although the information from each transducer can be used on its own, we show that their combined analysis permits a more robust identification and analysis of crude oils. The three transducers in the form of chips are interrogated with optical fiber reflectance probes, visible and NIR light sources, and CCD spectrometers and can be used either in a static (i.e., diving the chip transducers in the fluids) or in a dynamic flowing mode, this latter compatible with their microfluidic integration. The design and mode of operation of fluidic cells and measuring platforms suitable to work with each type of chip transducer are also described. In particular, the integration in a flow line of a NIRM working in transflectance geometry, together with an IT located in a separated optofluidic cell has enabled the real time characterization of oils, fractions and their mixtures in dynamic conditions.

The ability of the sensor systems to respond to dynamic changes in fluid composition and to withstand harsh environments (i.e., corrosion, high pressure, and temperature) similar to those existing in drilling wells, suggest that they might be used to monitor oil flows during extraction or in refineries, this latter for a direct identification of distillation products and mixtures. For these applications, some of the components of the previously described sensor systems as light sources and CCD spectrometers could be replaced by laser or LED light sources and photodiode arrays, however the ITs and NIRM design, operation mode, and fundamental working principles will remain essentially the same. Sensor systems for oil well control based on this family of transducers could imply long optical fiber connections and harsh (chemical and mechanical) operation conditions. Therefore, signal attenuation and mechanical damage are critical factors to be taken into account in their design. Bearing in mind these limitations, we have designed and fabricated these interferometric transducers and NIR dielectric mirrors to maximize their reflectance, optical performance, fiber-coupling suitability, and to guarantee their compatibility and integration with mechanically protected standard petrochemical sensor holders.

In the next sections, we describe the operating principles of these photonic sensor systems and prove their accuracy, reliability and stability for oil and hydrocarbon identification. However, no attempts have been made to use chemometrics [29,33] or other statistical procedures of data handling to interpret the obtained results. We are convinced that their use will expand the possibilities of these sensor systems for the analysis of crude oils, a type of studies that will be the subject of future investigations.

2. Measuring platforms and oil samples

2.1. Measuring platforms

Two platforms have been utilized for fluid analysis in static and flow conditions. A scheme and a photograph of the static platform used for the *pillared-BM* and *porous-BM* transducers are presented in Fig. 1a and b. It consists of a holder for the optical transducer chip, a liquid reservoir and a bundle of optical fibers mounted in a XYZ translation stage connected to a light source and a spectrometer. In this static platform, the transducer chip is interrogated from the backside of the substrate supporting the transducer with an optical fiber bundle. Referring for example to the *pillared-BM,* the array of nanopillars is facing down dived in the liquid media inside the liquid reservoir. The light used for the interrogation is supplied by a VIS-NIR light source (StellarNet), reflected back at the IT, and collected by one thread of the optical fiber bundle. The reflected light is registered by a CCD spectrometer HRS-VIS-005 from Mightex, with a bandwidth of 390–780 nm. The XYZ translation stage is utilized to control the spot position of analysis (yellow color in Fig. 1a), thus selecting the region of the transducer that is interrogated. Illumination and light collection is made with bare ~1 m long optical

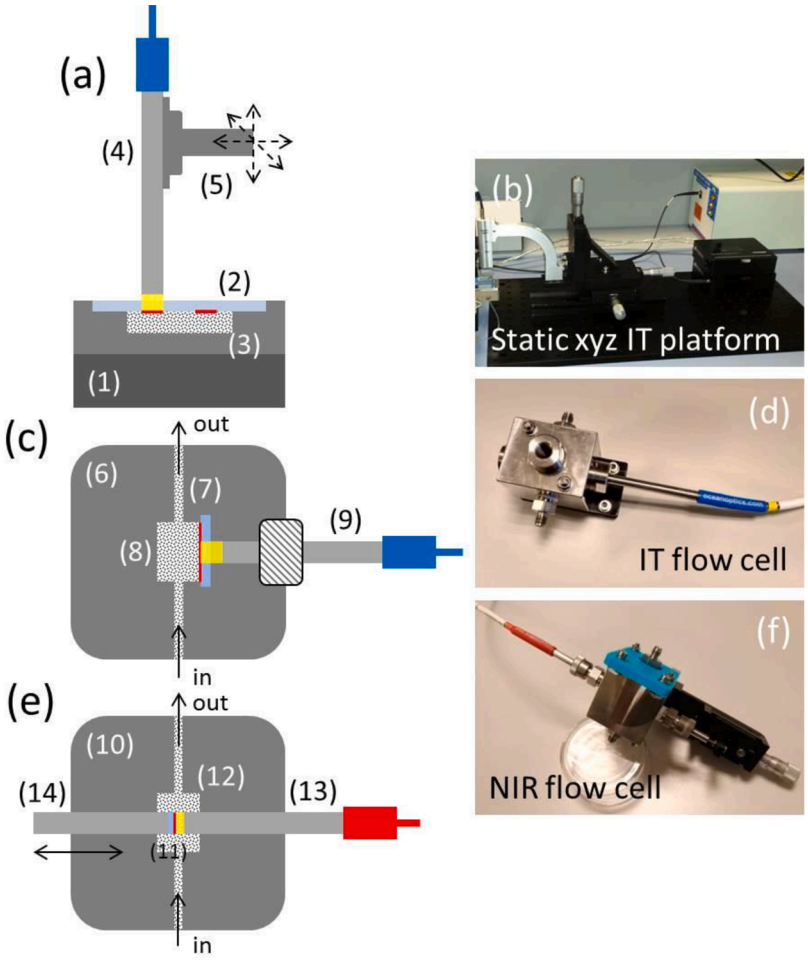

Fig. 1. Schemes (left) and photographs (right) of the measuring platforms/cells used for oil analysis. The location of the photonic transducers within each platform/cell is indicated in red. (a) and (b) Static platform. (1) holder, (2) transducer on fused silica plate, (3) liquid reservoir, (4) reflection probe, (5) XYZ translation stage. (c) and (d) Flow cell for porous-BM transducers, (6) stainless steel optofluidic cell, (7) transducer on fused silica window, (8) fluid channel and liquid chamber, (9) reflection probe. (e) and (f) Flow cell for NIRM transducers, (10) stainless steel optofluidic cell, (11) NIR mirror, (12) fluid channel and liquid chamber, (13) reflection probe, (14) movable stab. (For interpretation of the references to colour in this figure legend, the reader is referred to the web version of this article).

fibers.

The platform developed for fluid analysis in flow conditions was fabricated with two possible configurations (see the schemes and photographs in Fig. 1c–f) for either *porous-BM* or NIRM transducers (*pillared-BM* could be also used in the former configuration, provided that the pillared area of the substrate is large enough to do not entail focusing problems). These optofluidic cells are interrogated with suitable coaxial fiber optic reflection probes, light sources and spectrometers. They consisted of stainless steel cubes manufactured with several ports. In this design, two aligned ports are set for liquid inlet and outlet, and a third one to place a window (optical grade fused silica disc with 10 mm diameter and 1 mm thickness) for optical interrogation.

In a first configuration, the *porous-BM* transducer layer was directly deposited on a fused silica window and mounted in such a way that the active porous multilayer structure is immersed in the fluid when it circulates through the optofluidic cell. The reflection probe is placed in front of the backside of the deposited window. In this case, the optical system for signal collection consisted of a two meters long QR200-7-UV–vis reflection probe, a DH-2000-BAL UV–vis light source, and a CCD Maya 2000 Pro spectrometer, all from Ocean Optics.

In a second configuration, the NIRM transducer was placed onto a movable stab located in a port of the optofluidic cell facing the reflection probe. The distance between the NIRM and the reflectance fiber probe was varied to select the optical pathlenght inside the optofluidic cell and, therefore, the magnitude of the absorbance of the analyzed fluid. After signal optimization, this parameter was set to ~75 μm (i.e., a total optical pathlength of ~150 μm in transflectance mode). Two meters long QR200-7-VIS-NIR reflection probe, a HL-2000 NIR lamp, and a CCD NIRQuest monochromator, all from Ocean Optics, were used for the corresponding transflectance analysis.

The cells were connected by Swagelock 1/8" tube fittings. The liquid flowing through the inner volume of the cells was circulated from a thermostatic and stirred fluid reservoir (20 ml) under the thrust of a peristaltic pump (Spetec Perimax 16 Antipuls). A syringe-dosing pump (WPI AL1000-220) connected to the fluid reservoir was used for dynamic mixing experiments. After each set of measurements, the flow circuit, tubing system, cells, and optical components were cleaned circulating pure hydrocarbons. All the measurements reported in this paper were carried out at 45 °C and atmospheric pressure.

2.2. Reference hydrocarbons, crude oils and fractions

Several dead crude oil samples (i.e., without dissolved methane, numbered from *O1* to *O13*) and crude oil fractions obtained by distillation (*F1* to *F7*) were provided by the REPSOL Company and analyzed following the procedures described in Sections 3.3, 4 and 5. Table 1 gathers the complete set of crude oils and fractions used in the present study. They are characterized by a nominal density (at 20 °C and atmospheric pressure) and the partition of constituent hydrocarbons classified by their chain lengths in the ranges C1-C5, C6-10, C11-C15, C16-C20 or > C20 (this latter accounts for hydrocarbons with more than 20 C units, and identified with CW). Data collected in this table were also provided by REPSOL. Crude oils densities might be affected by uncertainties in the order of ~1−2 % of the reported values due to changes in the hydrocarbon content during their manipulation in the laboratory (e.g., partial evaporation of the lightest hydrocarbons or inhomogeneity in the most viscous oils). This series of examined oils and fractions covers the common standard range of densities and viscosities

Table 1
Nominal density (ρ) (at 20 °C), and carbon chain distribution of crude oils and fractions used in this work (CW represents hydrocarbons with more than 20 C units).

Oil/ Fraction	Nominal density ρ (g/cm^3)	Carbon chain distribution (%)				
		C1-C5	C6-C10	C11-C15	C16-C20	CW
O1	0.870	1.1	17.1	18.0	14.6	49.2
O2	0.939	2.6	10.5	6.8	11.7	68.4
O3	0.910	1.8	12.8	11.6	9.3	64.5
O4	0.959	0.3	6.9	9.6	14.4	68.8
O5	0.800	2.5	27.7	23.4	16.3	30.1
O6	1.021	0.0	1.2	4.5	8.9	85.3
O7	0.925	2.4	9.9	6.2	11.0	70.5
O8	0.921	1.8	12.8	11.6	9.3	64.5
O9	0.866	1.4	14.2	15.1	12.9	56.5
O10	0.960	0.5	7.6	8.4	15.1	68.4
O11	0.893	0.1	4.2	23.5	25.5	46.8
O12	0.876	–	–	–	–	–
O13	0.913	0.8	5.6	13.7	14.3	65.6
F1	0.837	0.0	33.6	66.4	0.0	0.0
F2	0.876	0.0	0.0	69.2	30.6	0.2
F3	0.911	0.0	0.0	0.5	62.4	37.1
F4	0.935	0.0	0.0	0.0	1.9	98.1
F5	0.976	0.0	0.0	0.0	1.5	98.5
F6	0.993	0.0	0.0	0.0	0.0	100.0
F7	1.001	0.0	0.0	0.0	0.0	100.0

of stabilized liquid oils. Pentane, hexane, heptane, octane, cyclohexane, cyclooctane, and toluene, (Sigma Aldrich; purity better than 99 %) were used as reference liquid hydrocarbons. Their nominal refractive indices and density values (at 20 °C and atmospheric pressure) were taken from the product technical data sheets provided by the supplier. Due to the fact that all measurements were carried out at 45 °C, these nominal values were corrected by specific temperature coefficients described in the literature for oils, hydrocarbons and solvents [34–36]. Finally, and as we report in the Supporting information (see Fig. S1), this set of reference hydrocarbons show linear correlations between their nominal refractive index *n* and the so-called *function of the refractive index* [15] (FRI = $(n^2\text{-}1)/(n^2\text{+}2)$) and their nominal densities through the well-known Lorentz-Lorenz relation [37,38].

3. Photonic transducers, stability in harsh conditions and operating principle

3.1. Morphology and optical properties of photonic transducers

The *pillared-BM* transducers were formed by arrays of nanopillars (200-250 nm diameter, 2000 nm height, 500 nm pitch) lithographed onto an area of 2 × 2 mm of a fused silica substrate. Each nanopillar consisted of a Bragg microcavity formed by two Bragg reflectors of 5 periods of Si_3N_4/SiO_2 compact bilayers (97 and 110 nm thickness, respectively) with a resonant cavity of SiO_2 (200 nm thickness) in between. A detailed description of their lithographic fabrication procedure can be found in ref. [22]. Fig. 2a shows a scanning electron microscope (SEM) micrograph of the nanopillars array. A typical reflectance spectrum of the *pillared-BM* transducer is presented in Fig. 2b. It shows a reflectance window from about 480–560 nm with a resonant peak at 512 nm when measured in air. The position of this peak (and the overall spectrum) shifts when the space between nanopillars is filled with fluids with different refractive indices.

The *porous-BM* transducers are Bragg microcavities consisting of two Bragg reflectors with a HLHLHLH porous multilayer structure (H and L stand for high and low refractive index materials, TiO_2 and SiO_2, respectively) with a porous resonant cavity layer of SiO_2 in between. The void fraction of the multilayer structure was about 40–50 %. Each layer was formed by tilted nanocolumns with a lateral size of several tenths of nanometer separated by a continuous open mesopored structure extending from the surface up to the interface with the substrate. They were prepared by e-beam evaporation in an oblique angle configuration where the substrate normal forms an angle of 70° with the direction of the deposited particles [26,27]. Fused silica discs (10 mm diameter, 1 mm thick) were used as substrates for the preparation of these transducers, although some preparations were also made on flat polished silicon wafers for an easy cross section SEM observation of their microstructure. A thorough description of these *porous-BM* transducers can be found in previous works [25,26,28]. It is noteworthy that the wavelength dependent reflectance of these *porous-BM* depicts a resonant peak, whose position is modulated by the refractive index of the fluid infiltrated within the open pores. Cross-section SEM micrographs of this photonic structure and a typical reflectance spectrum are presented in Fig. 2c and d. These SEM micrographs clearly show the high porosity of this layered structure, while its reflectance depicts the corresponding Bragg reflection band from about 460–650 nm and a resonant transmission peak at ~530 nm. Similarly to the *pillared-BM* transducers, the position of this feature red-shifts when the pores of the multilayer structure are filled with liquids of increasing refractive indices. For the purposes of the present work, it is of relevance that this photonic structure can be prepared in the form of a chip homogeneously deposited over an area up to 1.5 × 1.5 cm^2 on any kind of substrate, including transparent fused silica or onto an optical fiber tip.

NIRM transducers are highly reflective surfaces in the 800–2500 nm wavelength range. Most common surfaces used as NIR reflectors are made of evaporated gold mirrors (typical thickness higher than 100 nm) [39,40]. In this work we propose the use of dielectric mirrors formed by stacking layers of SiO_x (x<<1) and SiO_2 [41,42]. These two materials are transparent in the NIR region and when stacked in a structure of successive layers they behave as a Bragg mirror in the NIR region due to their high refractive index contrast (typically SiO_2 and SiO_x refractive indices are about 1.45 and 3.2 respectively, this latter very much dependent on its oxygen content [43]). These dielectric mirrors present two main advantages compared to conventional metallic mirrors. On the one hand, they can be tailored manufactured to show an optimized reflectance in a selected wavelength range. On the other hand, they provided the high chemical resistance required for a long standing analysis of crude oils. The SiO_x/SiO_2 NIR transducers used in the present work consisted of a multilayer of 12 layers of $SiO_{0.3}$ and SiO_2 prepared by magnetron sputtering deposition, respectively without and with 25 % oxygen incorporated in the main plasma gas (Ar at a pressure of 5.0 10^{-3} mbar). The deposition was made at a power of 225 W with an Advance Energy Pinnacle Plus power supply operated in pulsed mode (120 Hz). The cross section SEM micrograph and reflectance spectrum of a NIRM transducer are presented in Fig. 2e and f. In this case, the optical design of the NIRM transducer was optimized for the 1300–1800 nm wavelength range (i.e., to cover the O—H and C–H vibrational overtone bands). As an example, this figure also includes the absorption spectrum of heptane to illustrate the possibilities provided by these NIR selective mirrors to record transflectance spectra of hydrocarbons and crude oils.

SEM micrographs of the different transducers were acquired with a scanning electron microscope, Hitachi S4800 SEM-FEG, operated at 15 kV. The cross section micrographs were taken for the transducers deposited onto flat polished silicon wafers after dicing for cross section observation. The reflectance spectra of the *porous-BM* and *pillared-BM* interference transducers and that of the NIRM transducer shown for illustration in Fig. 2 were recorded in air (i.e., without exposing the transducers to liquids). It is also noteworthy that the particular shape and position of the resonant peak in the two ITs changed when modifying the thickness and the number of layers in the multilayer stack [44,45] or the pitch size in the array of nanopillars, for the *pillared-BM*.

3.2. Endurance test of the interferometric transducers at high temperature and hyperbaric conditions

To check the endurance of the ITs under conditions similar to those

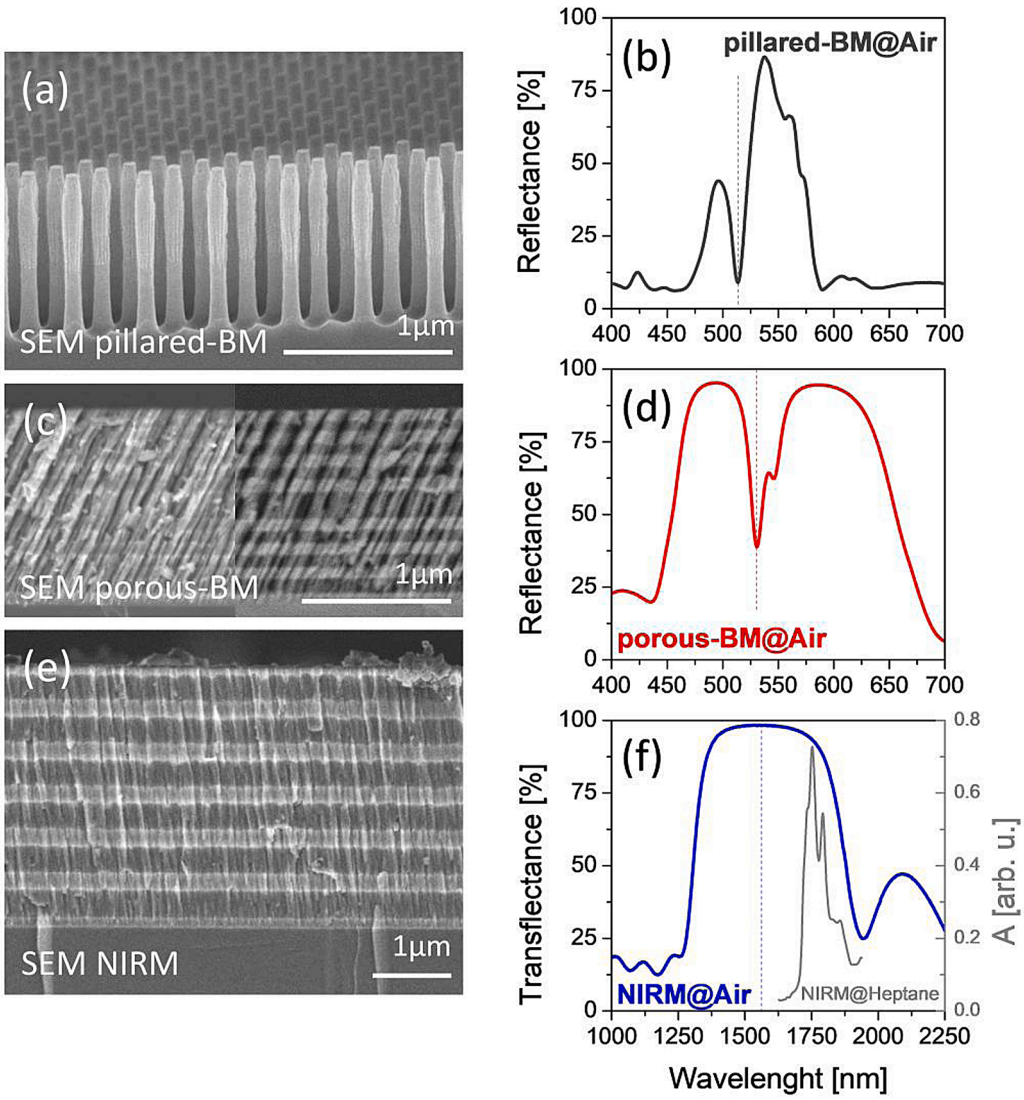

Fig. 2. SEM cross section micrographs (left) and reflectance spectra in air (right) of the photonic transducers. (a) and (b): Pillared-BM. (c) and (d): Porous-BM. Two SEM micrographs are shown collected with secondary (left) and back-reflected (right) electrons. (e) and (f): NIRM transducer. The absorption spectrum of heptane is included in (f) for comparison purposes.

found in real crude oil facilities, we have evaluated the performance of the *pillared-BM* and *porous-BM* transducers (the NIRM are compact dielectric multilayers with a proved stability at high pressure and elevated temperatures) before and after keeping them under high pressure and temperature in a hyperbaric chamber filled with crude oil at 150 °C and 800 bars for 14 h. Once all elements were inside the chamber, the temperature was slowly increased until reaching the selected high temperature and pressure conditions. As reported in SI (Fig. S2) both *pillared-BM* and *porous-BM* transducers were operative after the high temperature and pressure test immersed in crude oil in a hyperbaric chamber. It is worth mentioning that minor resonant peak position drifts were observed before and after the test, most probably due to the fact that either the measurements were not taken at exactly the same position on the transducer area or to minor differences in cleanness of the transducer after de hyperbaric test. Note that this is not a major issue because, as we will show below, the interpretation of the response of these transducers is always done in relative terms after calibration, i.e., only peak shifts (with respect to a reference) are considered and not their actual absolute positions.

3.3. Analysis of reference liquid hydrocarbons with ITs

The calibration procedure is exemplified in Fig. 3. Fig. 3a shows a series of reflectance spectra recorded for several reference liquid hydrocarbons brought in contact with the *porous-BM* transducer. The position of its resonant feature shifts to larger wavelengths as the refractive index of the liquid hydrocarbon increases. According to the effective medium theory [46], this shift stems from the filling of the open porosity in the *porous-BM* (or the empty space between nanopillars in the *pillared-BM*) with liquids of different refractive indices. Fig. 3b shows the evolution of the resonant peak position of the IT with respect to the nominal refractive index *n* of selected reference hydrocarbons (pentane, hexane, octane, cyclohexane, cyclooctane and toluene), demonstrating that there is a linear correlation between them. An alternative way to show this dependence when the shifts in the peak position are small is to represent the reflectance at a fixed wavelength vs. *n*. This is also done in Fig. 3b for the evolution of the reflectance values at 605 nm with *n* for the reference hydrocarbons. A similar linear correlation was found when the analysis was carried out with the *pillared-BM* transducers (see Fig. S3). For the particular transducer used in the experiment in Fig. 3, the slope of the plotted line defines the transducer sensitivity that, in this case, was 138 nm/RIU (RIU: refractive index units). A similar analysis

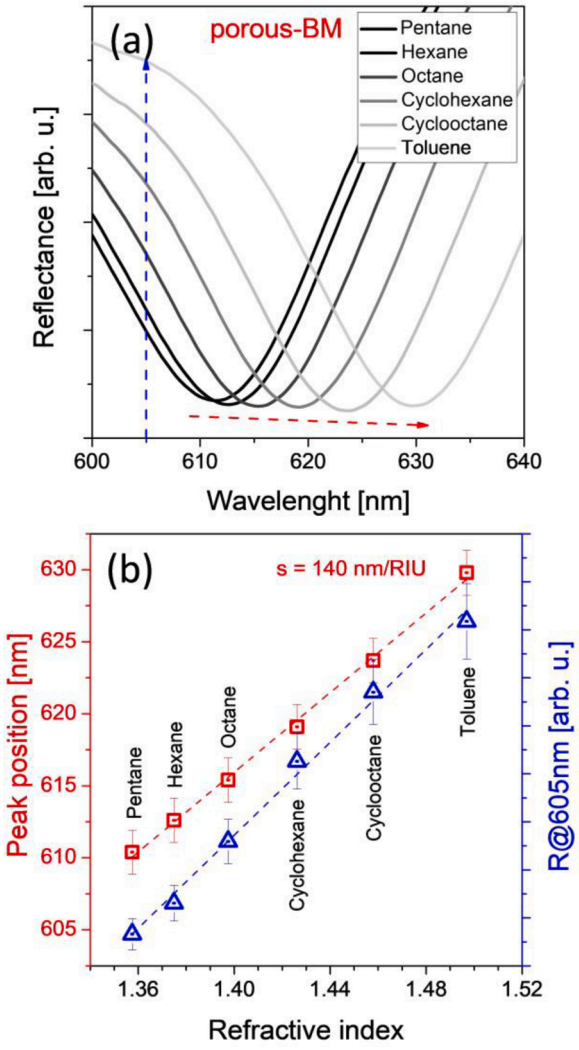

Fig. 3. (a) Reflectance around the resonance peak of a porous-BM transducer when it is brought in contact with several reference liquid hydrocarbons (i.e., pentane, hexane, octane, cyclohexane, cyclooctane and toluene). The arrows illustrate the effect of increasing the hydrocarbon refractive index. (b) Resonant peak position (left axis) and reflectance at 605 nm (right axis) vs. nominal refractive index of the reference liquid hydrocarbons. The linear regressions to these data (dashed lines) render the calibration for this transducer.

carried out with the *pillared-BM* transducer (see Fig. S3b) rendered a sensitivity of 295 nm/RIU. In the curse of this investigation, it was realized that IT transducers may change their response due to contamination and other uncontrolled effects and that calibration was needed before each experimental identification analysis of crude oils and/or fractions or after long time (several months) IT storage in air. For the sake of simplicity, and taken into account the linear correlation between resonant peak positions and the nominal refractive index values for these reference hydrocarbons, calibration tests were usually done with two pure hydrocarbons with quite different nominal refractive index values, generally hexane and toluene.

For the present analysis, we have neglected the refractive index chromatic dispersion, i.e., the variation of refractive index vs. wavelength, of the liquid hydrocarbons. This chromatic dispersion in the visible is about $\sim 5 \cdot 10^{-5}$ RIU/nm, meaning that the maximum error between the lowest and highest refractive index hydrocarbons depicted in Fig. 3 (with a refractive index difference of 0.15 RIU), as determined with the procedure outlined above, is about $1.5 \cdot 10^{-3}$ RIU, i.e., below the 1 % of the measured value. This might be important when comparing the results obtained in this work with other refractive index values reported in the literature that, obtained with conventional apparatus based on the Abbe method, correspond to the refractive index at a fixed wavelength at 589.3 nm due to the emission line of sodium [15].

4. Crude oils and fractions identification with ITs

4.1. Fractions analysis with ITs

Identification and indirect determination of density and other characteristics of unprocessed crude oils and fractions through the correlation of these magnitudes with their refractive indices determined with conventional Abbe refractometers may be hampered by the high intrinsic absorption of crude oils in the visible region of the spectrum even if using little volumes of sample (in the range of 10^{-3} l) [15–17]. This problem does not affect the ITs utilized in the present work where the actual amount of liquid required to get the photonic response in reflection mode is very low (i.e., around 10^{-9} l, just the volume required to fill either the empty space between nanopillars in the *pillared-BM* or the void fraction in the *porous-BM*, where it enters by mere infiltration into the active analysis zone of the transducers). The calibration results in Fig. 3 and the linear correlation between the refractive index and density of reference liquids (see Supporting information, Fig. S1), clearly validate the use of the IT for identification of pure hydrocarbons. The question is now whether a similar correlation holds for oil fractions, in the form of a homogeneous liquid phase, or crude oils, generally consisting of a heterogeneous emulsion. Fig. 4a and c shows the reflectance spectra around the resonant peak for the *pillared-BM* and *porous-BM* transducers dived in six different fractions taken as problem examples, and hexane and toluene taken as references for calibration.

Fig. 4b and d shows plots of the recorded resonant peak position vs. the nominal density of the fractions and reference hydrocarbons. The plots of the resonant peak positions for the *pillared-BM* and *porous-BM* vs. the density of the fractions depict a linear correlation, which enables both the identification and classification of the examined fractions in case that they were supplied as unknown samples. It is interesting that the slopes of the linear regressions in Fig. 4b and d differ for each transducer, indicating a distinct sensitivity. From the two sets of measurements in Fig. 4, the resonant peak position sensitivities determined from the calibration with the two pure hydrocarbons were 154 nm/(gr cm^{-3}) and 89 nm/(gr cm^{-3}) for these particular *pillared-BM* and *porous-BM* ITs, respectively. The higher sensitivity of the former agrees with the relatively larger open space between the nanopillars available for liquid infiltration.

Considering the linear correlation between the nominal refractive index and resonant peak positions of the reference hydrocarbons, it is also possible to assess experimental refractive index parameters ($n_{porous\text{-}BM}$ or $n_{pillared\text{-}BM}$, for *porous-BM* or *pillared-BM* transducers, respectively) for each fraction. We should note that these experimental refractive index parameters are considered as identifying parameters related to the fluid nominal refractive index (see next section). The corresponding plots of resonant peak positions vs. the calculated $n_{porous\text{-}BM}$ or $n_{pilllared\text{-}BM}$ values are reported in the Supporting information Fig. S4).

4.2. Fractions vs. crude-oils analysis with IT transducers

The analysis of oil fractions, characterized by a homogenous liquid phase, rendered equivalent results with the two IT transducers as evidenced by the linear correlation found when representing and comparing the resonant peak position of one transducer against that of the other for the different examined fractions (see Supporting information, Fig. S5). This equivalence when analyzing homogeneous liquids is further highlighted in Fig. 5a showing a linear correlation when representing the nominal densities of the fractions (Table 1) and the variation in the experimental refractive index parameters (see Fig. S4) with respect to the values obtained for fraction *F1 (i.e.,* $\Delta n_{porous\text{-}BM}$ *(Fn)* = $n_{porous\text{-}BM}$ *(Fn)* - $n_{porous\text{-}BM}$ *(F1)* and $\Delta n_{pillared\text{-}BM}$ *(Fn)* = $n_{pillared\text{-}BM}$ *(Fn)* -

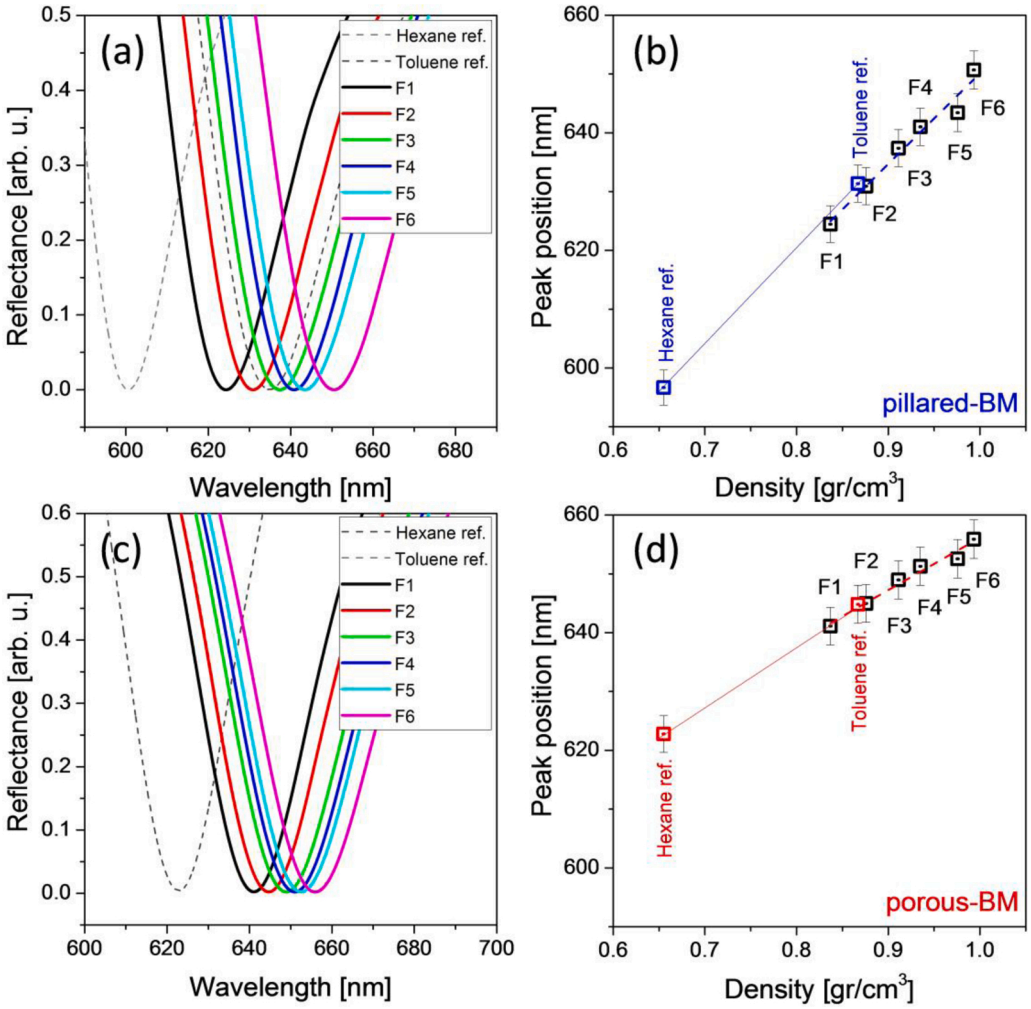

Fig. 4. Reflectance spectra around the resonant peak of pillared-BM (a) and porous-BM (c) transducers for six crude-oil fractions and two reference hydrocarbons (hexane and toluene), and plots of the corresponding resonant peak positions vs. nominal densities for the pillared-BM (b) and porous-BM (d) transducers.

$n_{pillared\text{-}BM}$ (*F1*)) for the two ITs. However, Fig. 5c shows that a similar plot of density vs. $\Delta n_{porous\text{-}BM}$ and $\Delta n_{pillared\text{-}BM}$ for the analyzed crudes depicts a larger dispersion of data points suggesting that the two transducers behave differently when analyzing multiphase crudes. We may assume that the solid particles suspended in some crude-oils will not enter readily in the open porosity of the *porous-BM* transducer, while they will do into the channels between the pillared structure of the *pillared-BM*. Similarly, the large molecules contributing to increase the viscosity of crude oils may either be unable to diffuse into the *porous-BM* or, if they do, they may remain inside the porous multilayer preferentially to lighter components that may diffuse out more readily. Whatsoever is the reason for the different response of the two interferometric transducers when analyzing multiphase liquids, the information retrieved from them can be considered complementary. Fig. 5c shows that the distribution of data points for the *porous-BM* is more scattered than that for the *pillared-BM,* in general overestimating the refractive index parameters of crude oils with respect to that of fractions, with some exceptions for heavier crudes. Similar tendencies can be observed when plotting the $\Delta n_{pillared\text{-}BM}$ values measured for the *pillared-BM* against the equivalent magnitude $\Delta n_{porous\text{-}BM}$ determined with the *porous-BM* both for the fractions (Fig. 5b) and the crude oils (Fig. 5d). Another interesting outcome of the representation in Fig. 5c is that the use of the two IT transducers together will permit to distinguish crude-oils with similar density and different ratio between soft and viscous-solid components. As an example, the dots with full symbols in Fig. 5c and d correspond to the crudes *O1* and *O9* which, according to Table 1, have very close density values of 0.870 g/cm^3 and 0.866 g/cm^3 but quite different variation of the refractive index parameter for each transducer, a feature enabling a straightforward identification of the two crude oils. Other examples could be also identified in these plots.

From a general perspective, although we cannot claim that the experimental refractive index parameters $n_{porous\text{-}BM}$ and $n_{pillared\text{-}BM}$ determined with the two ITs correspond to true values of refractive index of the crude-oil, the reproducibility of results and the systematic variation of resonant peak position (i.e., evolution of $\Delta n_{pillared\text{-}BM}$ and $\Delta n_{porous\text{-}BM}$ values) provide a clear way of identifying crude oils and fractions. In this regard, it is remarkable that the scattered distribution of data points in Fig. 5c defines a similar margin of error than other analysis in literature based on refractive index values determined with the conventional Abbe method [15] (see Supporting information Fig. S6). This consideration also applies to the *refractive index function*, FRI = $(n^2\text{-}1)/(n^2\text{+}2)$, which uses to be correlated with other properties of crude oils such as density or viscosity [15–17]. For example, a rather common relationship between FRI and density values is the so-called one-third rule, referring that the FRI to density ratio approaches 1/3 for a large number of crude oils and fractions (deviations from this ratio are the subject of active discussion) [15]. Although in our analysis we rely on differences in $\Delta n_{porous\text{-}BM}$ or $\Delta n_{pillared\text{-}BM}$ rather than in the absolute values of $n_{porous\text{-}BM}$ or $n_{pillared\text{-}BM}$, it is remarkable that the FRI to density ratios calculated with the experimental $n_{porous\text{-}BM}$ or $n_{pillared\text{-}BM}$ parameters rendered values in the range of 0.29–0.32 and 0.28–0.33 for the *porous-BM* and *pillared-BM* transducers, respectively. In this way, the

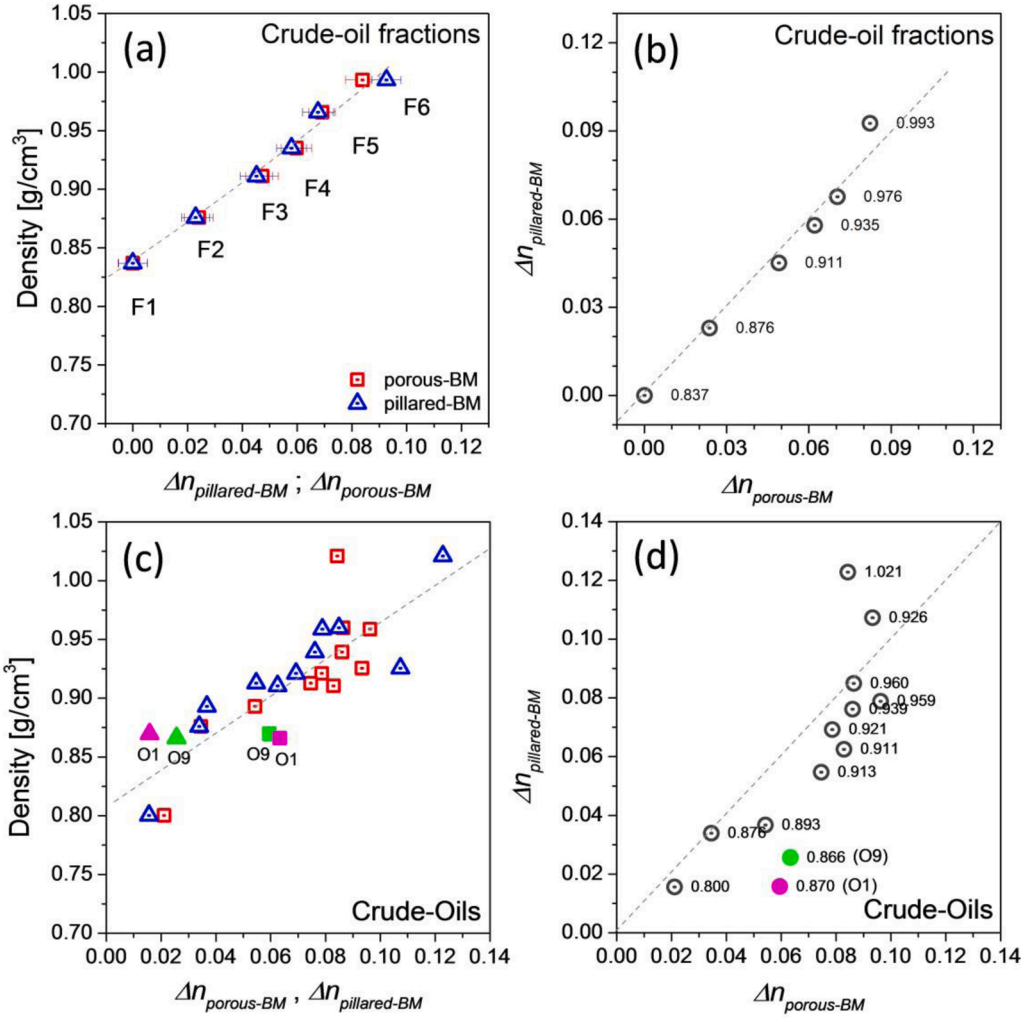

Fig. 5. Plots of the nominal density of the fractions (a) and crude oils (c) in Table 1 vs. their relative refractive index parameters, $\Delta n_{porous\text{-}BM}$ (red squares) and $\Delta n_{pillared\text{-}BM}$ (blue triangles). Correlation between $\Delta n_{pillared\text{-}BM}$ and $\Delta n_{porous\text{-}BM}$ obtained for the fractions (b) and crude oils (d). Nominal density values at 20 °C for each fraction/crude oil are included in these plots. The dashed lines included in the four panels correspond to linear regressions. Full symbols in (c) and (d) correspond to two oils with similar nominal density but different $\Delta n_{pillared\text{-}BM}$ and $\Delta n_{porous\text{-}BM}$ values, thus enabling their straightforward identification. (For interpretation of the references to colour in this figure legend, the reader is referred to the web version of this article).

rather similar value of this ratio determined for the two IT transducers support that the analysis is as reliable as that using other conventional methods to determine the refractive indices of crudes.

5. Oil identification with NIRM transducers

NIR spectroscopy is a classical method for the analysis of liquids with many application examples available in the literature, including the identification and analysis of hydrocarbons and crude oils [29,32]. A preliminary study of pure hydrocarbons in the flow cell with the developed NIRM transducers reveals differences in the relative intensities of the characteristic C–H first overtone bands around 1650−1850 nm (see, for example, Fig. S7 in SI and similar results obtained in a conventional NIR spectrometer in ref. [29,30]) that can serve to identify pure hydrocarbons and their mixtures with the help of machine learning procedures based on multivariate analysis [29,40]. In relation with the purposes of the present work, this preliminary analysis and the spectra in Fig. S7 prove that NIRM transducers can be effectively used for pure hydrocarbon identification. Although it is not the objective of the present work devoted to oil identification, it is noteworthy that NIRM transducers can be also used for the detection of emulsified water and other components of oil as exemplified in Supporting information Fig. S8 showing a series of transflectance spectra recorded for the *O5* crude oil with increasing amounts of water up to a 3.0 vol%.

However, NIR spectra recorded for selected crude oils from different sources and physical properties present extra features if compared with respect to the spectra acquired for pure hydrocarbons. Fig. 6a shows transflectance spectra in the 1300−1900 nm wavelength range of five crude-oil samples. Two regions can be clearly distinguished in these spectra. A first region in the 1300−1600 nm range depicts a broad loss of intensity that is enhanced for the shortest wavelengths. The background-like curves in this region derive from the tails of the broad absorption bands of these crude oils extending from the visible and/or from particle light scattering phenomena commonly associated with the existence of a high concentration of asphaltene particles in the crude oil suspension [30,31]. The quantification of these background-like curves in the 1300−1600 range provides a first means for the identification of crude oils. Thus, when representing the absorbance recorded with the NIRM transducer (i.e., log(1-T)), the resulting plots (see inset in Fig. 6a) are linear in the 1300−1600 nm wavelength range and their slope may be taken as an identifying parameter of the crude oils under analysis. It must be stressed that, for a fixed optical pathlength in a transflectance analysis, this *scattering slope parameter* S_{SC} is a robust measurement of the light scattering properties of the crude oil. On the other hand, a second region of interest that can be identified in the transflectance spectra corresponds to the 1650−1850 nm range, where the signature of the C–H first overtone absorption bands of the hydrocarbons and crude oil develops. In this case, unlike what is observed with pure hydrocarbons (Fig. S7), the recorded C–H fingerprints of the selected crude oils are very similar to each other and appear distorted by the absorption/dispersion background-like band described above. The small differences in the shapes of the recorded C–H first overtone band for crude oils from quite different sources and characteristics is due to the fact that oils are complex mixtures of many (tens!) of hydrocarbons. Fig. 6b shows the

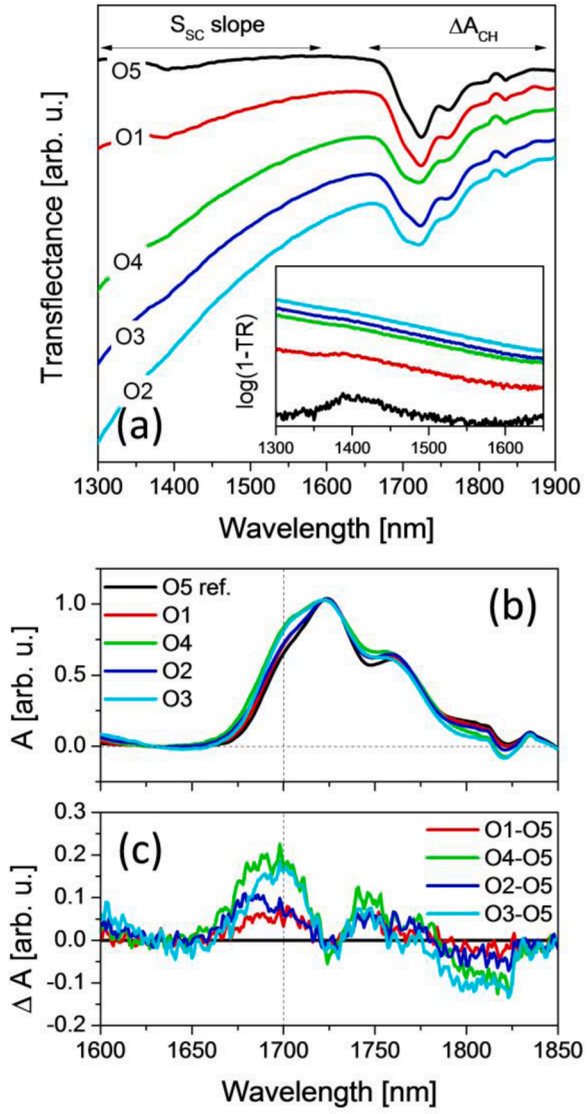

Fig. 6. Transflectance analysis of crude oils recorded with the NIRM transducers. (a) Experimental spectra of selected crude oils (O1 O2, O3, O4 and O5 in Table 1). The regions considered for the determination of S_{SC} and ΔA_{CH} parameters are indicated. (b) Normalized absorbance (top) and On-O5 difference spectra (bottom) in the NIR first overtone region of −CH bonds.

absorbance spectra of five crude oils (*O1-O5*) in the 1650 and 1850 nm range after background subtraction and normalization. The difference spectra with respect to a reference sample (in this case we take as reference the crude oil with the lowest nominal density and dispersion losses of the series, i.e., sample *O5*) $\Delta A_{sample} = (A_{sample} - A_{ref})$ reveals a noticeable feature at 1660−1720 nm, which varies in shape and intensity for the examined crude oils. We propose to use the intensity of this feature ΔA_{CH} as a second identifying parameter of crude oils analyzed with the NIRM transducers.

To prove the reliability of these NIRM parameters for crude oil identification, the determined S_{SC} and ΔA_{CH} values have been correlated with characteristic properties of the crude oils as their nominal density and proportion of carbon chains larger than 20 units (see Table 1), as well as with the relative refractive index parameter determined with the porous-BM transducers, $\Delta n_{porous\text{-}BM}$. Fig. 7 shows a series of plots where nominal density, proportion of long chain hydrocarbons (larger than 20 C units, CW in Table 1) and $\Delta n_{porous\text{-}BM}$ values are represented against the values of these two NIRM identifying parameters for crudes *O1* to *O5*. This series of samples was selected as a set of representative crude

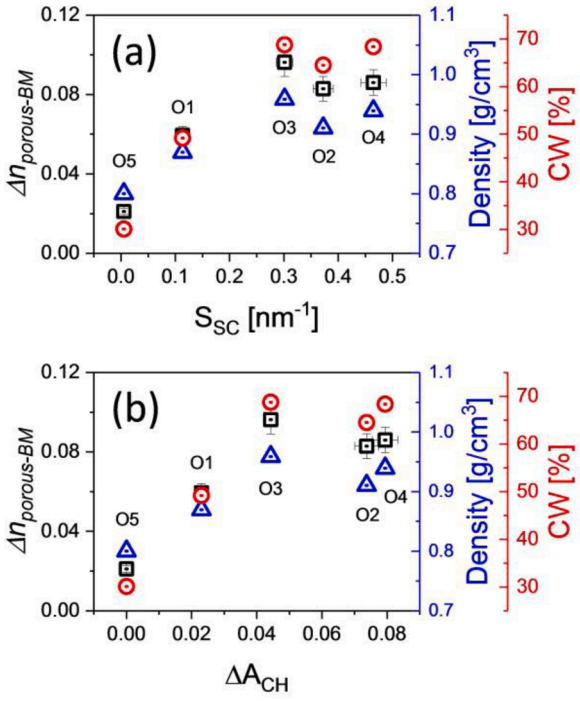

Fig. 7. Plots of experimental $\Delta n_{porous\text{-}BM}$ (black squares) and nominal density (blue triangles) and CW (red circles) of selected crude oils (O1-O5, see Table 1) against the scattering slope S_{SC} (a) and differential intensity ΔA_{CH} (b) parameters obtained from data recorded with the NIRM transducer. (For interpretation of the references to colour in this figure legend, the reader is referred to the web version of this article).

oils of the total available samples. Nominal density and carbon chain distribution values of crudes *O1* to *O5* cover the range of the collection of oil samples in terms of viscosity, optical dispersion and optical absorption. Also, they are optimal for flow conditions measurements and combined optical analysis by IT and NIRM techniques. Fig. 7a shows that $\Delta n_{porous\text{-}BM}$, as well as the nominal density and *CW* content increase as the scattering slope parameter (S_{SC}) takes values of ~0.3 nm^{-1}. For larger slope values, these parameters remain about constant. Fig. 7b shows a similar qualitative behaviour, with rising $\Delta n_{porous\text{-}BM}$, density and *CW* values until the differential intensity ΔA_{CH} gets ~0.04 and minor differences for larger ΔA_{CH} values. The direct correlations emerging from these plots support the congruence of data taken with the two types of photonic sensors and show that the simultaneous use of interferometric and NIMR transducers would reinforce the identification capacity of crude oils with the possibility to assess crude oil properties such as density and proportion of long chain hydrocarbons.

It is also noteworthy that the combined analysis with several transducers outlined above permits to assign several independent experimental parameters to each crude oil ($\Delta n_{porous\text{-}BM}$, S_{SC}, and ΔA_{CH}), supplying complementary information for their identification. Therefore, from this series of representations it appears that each crude oil sample can be identified unambiguously and that clear correlations can be established between the corresponding experimental parameters and nominal properties of the crudes.

6. Analysis of oil mixtures in flow conditions

The advantages of IT and NIRM transducers for the flow analysis of crude oils are further evidenced when they are used in series within a flow-loop circuit. To illustrate the capabilities of the simultaneous analysis with *porous-BM* and NIRM transducers, we present an evaluation analysis of a varying *O1/O4* crude-oil mixture, starting with 15 mL of pure *O1* oil and progressively adding *O4* oil at a rate of 7.5 mL per

hour. The experiment lasted 2 h up to reaching an even *O1/O4* crude-oil mixture.

Fig. 8a shows a series of resonant peak spectra taken with the *porous-BM* transducer at different times and, therefore, corresponding to a different *O1/O4* ratio in the mixture. Fig. 8b shows that there is a linear correlation when representing the variation of the reflectance intensity at 705 nm and the values of the calculated $\Delta n_{porous\text{-}BM}$ parameter with respect to the *O1/O4* crude oil ratio in the mixture. This linear correlation sustains that this IT can be straightforwardly used for the analysis of crude oil mixtures.

On the other hand, Fig. 8c shows the series of NIR spectra plotted in absorbance scale that were recorded with the NIRM transducer in this mixing experiment. The normalized difference spectra are plotted in the inset of this figure. The evaluation of the slope in the 1300−1600 nm range and the intensity of the difference spectra at 1654 nm make possible to follow the crude-oil mixing process in real time. The plot in Fig. 8d shows that the S_{SC}, and ΔA_{CH} parameters linearly change with the *O4/O1* crude-oil ratio in the mixture. The linear character of the plots in Fig. 8b and d, each one obtained with a different type of transducer, confirms their complementarity and that their simultaneous use can improve the identification capacity of crude oils and mixtures (we must note that in other cases such a linear behavior might not hold if the volume of the mixture differs from that of their constituent according to specific mixing rules [47]).

7. Summary and conclusions

We have proved that crude oil identification can be successfully done using various types of photonic sensor systems. Two principles of detection relying on interference and direct transflectance approaches and three different transducer architectures have been tested with a large set of crude oils and fractions. The small size of the transducers and their compatibility with optical fibers sustain their potential implementation in the form of chips for "*in-situ*" analysis in oil wells and/or refinery streams, a possibility backed by the reproducibility of their response after immersion in oils at high pressure and temperature.

The first type of interference transducers working in the visible consists of nanopillar arrays or porous thin film multilayers of two materials with different refractive index, both of them depicting a Bragg microcavity behavior. They provide a direct correlation between the position of their characteristic resonant features and the refractive indices of pure hydrocarbon, distilled oil fractions or crude oils in which they are immersed. After calibration, the analysis of a large series of oils has revealed a direct correlation between measured relative refractive index parameters and the oil density, a dependence that can be used for oil identification. On the other hand, NIRM transducers, based on a multilayer structure made of silicon and silicon oxides layers, can be used for the recording of scattering and absorption features of crude oils and hydrocarbons in the NIR spectral region, together with that of other constituent of the mixture as emulsified water. Although recorded spectra show similar C–H overtone absorption bands when comparing

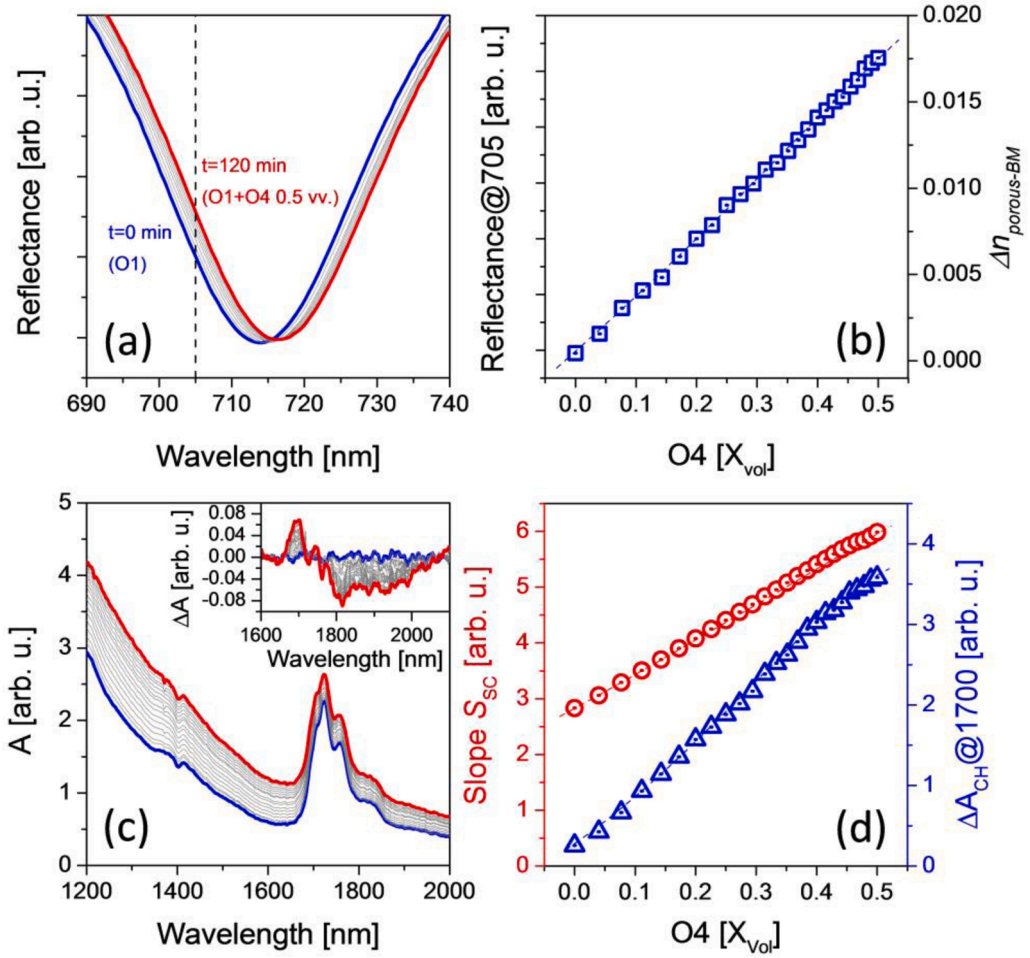

Fig. 8. Reflectance around the resonant peak acquired with a porous-BM transducer (a) and absorbance in the 1200-2000 nm range acquired with NIRM transducer (c) for a series of O1/O4 crude oil mixtures measured in flow conditions. Evolution of $\Delta n_{porous\text{-}BM}$ (b), scattering slope S_{sc} and intensity variation within first C-H overtone region ΔA_{CH} (d) as a function of the O4/O1 ratio in the crude-oil mixture.

different oils, it is proved that a careful analysis of the spectral shapes and of the broad absorption feature in the 1300−1600 nm range provides a powerful basis for oil identification and monitoring using this transducer. The two types of transducers have shown reliable results for identification of crude oils, fractions and mixtures in static and in flow conditions. This latter possibility opens the way for the direct monitoring of crude oils at extraction wells or for traceability purposes in refineries and similar facilities devoted to oil handling and processing.

CRediT authorship contribution statement

Jorge Gil-Rostra: Conceptualization, Methodology, Investigation, Analysis, Writing - original draft, Writing - review & editing. **Sergio Quintero:** Conceptualization, Methodology, Investigation, Analysis, Writing - original draft, Writing - review & editing. **Víctor Rico:** Methodology, Investigation, Analysis. **Francisco Yubero:** Conceptualization, Methodology, Analysis, Writing - original draft, Writing - review & editing. **Francisco J. Sanza:** Conceptualization, Methodology, Investigation, Analysis. **Rafael Casquel:** Conceptualization, Methodology, Investigation, Analysis. **Emilio Gallo-Valverde:** Validation, Project administration. **María E. Jara Galán:** Validation, Project administration. **Paula Sanz-Sanz:** Validation, Project administration. **Miguel Holgado:** Conceptualization, Methodology, Validation, Project administration, Funding acquisition, Supervision. **Agustín R. González-Elipe:** Conceptualization, Methodology, Writing - original draft, Writing - review & editing, Project administration, Funding acquisition, Supervision.

Declaration of Competing Interest

The authors declare that they have no known competing financial interests or personal relationships that could have appeared to influence the work reported in this paper.

Acknowledgments

This work was carried out within the frame of the project REMO (PR150060358) funded by INDRA and REPSOL. Transducers utilized in this work were in part developed in project HERON (TEC2017-84846-R) funded by the AEI, MICNN and EU-FEDER funds. The work of S.Q. was supported by the predoctoral contract by the Universidad Politecnica de Madrid, Madrid, sponsored by Banco de Santander under grant RR24/2017.

Appendix A. Supplementary data

Supplementary material related to this article can be found, in the online version, at doi:https://doi.org/10.1016/j.snb.2021.130265.

References

[1] J.G. Speight, The Chemistry and Technology of Petroleum, CRC Press, 2006, https://doi.org/10.1201/9781420008388.
[2] F.D. Mango, The light hydrocarbons in petroleum: a critical review, Org. Geochem. 26 (1997) 417–440, https://doi.org/10.1016/S0146-6380(97)00031-4.
[3] R.A. Kanaly, S. Harayama, Biodegradation of high-molecular-weight polycyclic aromatic hydrocarbons by bacteria, J. Bacteriol. 182 (2000) 2059–2067, https://doi.org/10.1128/JB.182.8.2059-2067.2000.
[4] J.M. Santos, A. Vetere, A. Wisniewski, M.N. Eberlin, W. Schrader, Comparing crude oils with different API gravities on a molecular level using mass spectrometric analysis. Part 2: resins and asphaltenes, Energies 11 (2018) 2767, https://doi.org/10.3390/en11102767.
[5] P.R. Filgueiras, C.M.S. Sad, A.R. Loureiro, M.F.P. Santos, E.V.R. Castro, J.C.M. Dias, R.J. Poppi, Determination of API gravity, kinematic viscosity and water content in petroleum by ATR-FTIR spectroscopy and multivariate calibration, Fuel 116 (2014) 123–130, https://doi.org/10.1016/j.fuel.2013.07.122.
[6] O. Abbas, C. Rebufa, N. Dupuy, A. Permanyer, J. Kister, PLS regression on spectroscopic data for the prediction of crude oil quality: API gravity and aliphatic/aromatic ratio, Fuel 98 (2012) 5–14, https://doi.org/10.1016/j.fuel.2012.03.045.
[7] J. Woods, J. Kung, D. Kingston, L. Kotlyar, B. Sparks, T. McCracken, Canadian crudes: a comparative study of SARA fractions from a modified HPLC separation technique, Oil Gas Sci. Technol. Rev. IFP 63 (2008) 151–163, https://doi.org/10.2516/ogst:2007080.
[8] A.G. Marshall, R.P. Rodgers, Petroleomics: the next grand challenge for chemical analysis, Acc. Chem. Res. 37 (2004) 53–59, https://doi.org/10.1021/ar020177t.
[9] B. Fuhr, K. Scott, H. Dettman, S. Salmon, Fractionation of bitumen by distillation, Sara analysis and gel permeation chromatography, Prepr. Am. Chem. Soc. Div. Pet. Chem. 50 (2005) 264–265.
[10] A. Gaspar, E. Zellermann, S. Lababidi, J. Reece, W. Schrader, Characterization of saturates, aromatics, resins, and asphaltenes heavy crude oil fractions by atmospheric pressure laser ionization fourier transform ion cyclotron resonance mass spectrometry, Energy Fuels 26 (2012) 3481–3487, https://doi.org/10.1021/ef3001407.
[11] O. Achugasim, I.E. Ekpo, Precipitation of heavy organics (asphaltenes) from crude oil residue using binary mixtures of n-alkanes, Adv. Chem. Eng. Sci. 5 (2014) 96–101, https://doi.org/10.4236/aces.2015.51010.
[12] S.I. Andersen, J.O. Jensen, J.G. Speight, X-ray diffraction of subfractions of petroleum asphaltenes, Energy Fuels 19 (2005) 2371–2377, https://doi.org/10.1021/ef050039v.
[13] S.I. Andersen, J.G. Speight, Thermodynamic models for asphaltene solubility and precipitation, J. Pet. Sci. Eng. 22 (1999) 53–66, https://doi.org/10.1016/S0920-4105(98)00057-6.
[14] S.I. Andersen, J.G. Speight, Petroleum resins: separation, character, and role in petroleum, Pet. Sci. Technol. 19 (2001) 1–34, https://doi.org/10.1081/LFT-100001223.
[15] H.W. Yarranton, J.C. Okafor, D.P. Ortiz, F.G.A. van den Berg, Density and refractive index of petroleum, cuts, and mixtures, Energy Fuels 29 (2015) 5723–5736, https://doi.org/10.1021/acs.energyfuels.5b01376.
[16] A.K. George, R.N. Singh, Correlation of Refractive Index and Density of Crude Oil and Liquid Hydrocarbon, 3, 2015, p. 3.
[17] M.R. Riazi, Y.A. Roomi, Use of the refractive index in the estimation of thermophysical properties of hydrocarbons and petroleum mixtures, Ind. Eng. Chem. Res. 40 (2001) 1975–1984, https://doi.org/10.1021/ie000419y.
[18] D. Chen, C. Jones, B. Dai, A. VanZuilekom, An assessment of neural networks in processing optical sensor measurements for advanced multi-analyte fluid characterization, International Petroleum Technology Conference (2020), https://doi.org/10.2523/IPTC-19756-MS.
[19] M. Fingas, C. Brown, Review of oil spill remote sensing, Mar. Pollut. Bull. 83 (2014) 9–23, https://doi.org/10.1016/j.marpolbul.2014.03.059.
[20] U.T. Nakate, P. Patil, R.N. Bulakhe, C.D. Lokhande, S.N. Kale, M. Naushad, R. S. Mane, Sprayed zinc oxide films: ultra-violet light-induced reversible surface wettability and platinum-sensitization-assisted improved liquefied petroleum gas response, J. Colloid Interface Sci. 480 (2016) 109–117, https://doi.org/10.1016/j.jcis.2016.07.010.
[21] T.A. Saleh, G. Fadillah, O.A. Saputra, Nanoparticles as components of electrochemical sensing platforms for the detection of petroleum pollutants: a review, TrAC Trends Anal. Chem. 118 (2019) 194–206, https://doi.org/10.1016/j.trac.2019.05.045.
[22] I. Cornago, A.L. Hernández, R. Casquel, M. Holgado, M.F. Laguna, F.J. Sanza, J. Bravo, Bulk sensing performance comparison between silicon dioxide and resonant high aspect ratio nanopillars arrays fabricated by means of interference lithography, Opt. Mater. Express 6 (2016) 2264–2272, https://doi.org/10.1364/OME.6.002264.
[23] A.L. Hernández, R. Casquel, M. Holgado, I. Cornago, F. Fernández, P. Ciaurriz, F. J. Sanza, B. Santamaría, M.V. Maigler, M.F. Laguna, Resonant nanopillars arrays for label-free biosensing, Opt. Lett. 41 (2016) 5430–5433, https://doi.org/10.1364/OL.41.005430.
[24] A.L. Hernández, R. Casquel, M. Holgado, I. Cornago, F.J. Sanza, B. Santamaría, M. Maigler, F. Fernández, A. Lavín, M.F. Laguna, Arrays of resonant nanopillars for biochemical sensing, Opt. Lett. 40 (2015) 2370–2372, https://doi.org/10.1364/OL.40.002370.
[25] M. Oliva-Ramirez, L. González-García, J. Parra-Barranco, F. Yubero, A. Barranco, A.R. González-Elipe, Liquids analysis with optofluidic bragg microcavities, ACS Appl. Mater. Interfaces 5 (2013) 6743–6750, https://doi.org/10.1021/am401685r.
[26] M. Oliva-Ramirez, A. Barranco, M. Löffler, F. Yubero, A.R. González-Elipe, Optofluidic modulation of self-associated nanostructural units forming planar bragg microcavities, ACS Nano 10 (2016) 1256–1264, https://doi.org/10.1021/acsnano.5b06625.
[27] A. Barranco, A. Borras, A.R. Gonzalez-Elipe, A. Palmero, Perspectives on oblique angle deposition of thin films: from fundamentals to devices, Prog. Mater. Sci. 76 (2016) 59–153, https://doi.org/10.1016/j.pmatsci.2015.06.003.
[28] M. Oliva-Ramírez, J. Gil-Rostra, F. Yubero, A.R. González-Elipe, Robust polarization active nanostructured 1D Bragg Microcavities as optofluidic label-free refractive index sensor, Sens. Actuators B Chem. 256 (2018) 590–599, https://doi.org/10.1016/j.snb.2017.10.060.
[29] M. Khanmohammadi, A.B. Garmarudi, A.B. Garmarudi, M. de la Guardia, Characterization of petroleum-based products by infrared spectroscopy and chemometrics, TrAC Trends Anal. Chem. 35 (2012) 135–149, https://doi.org/10.1016/j.trac.2011.12.006.
[30] F.S. Falla, C. Larini, G.A.C. Le Roux, F.H. Quina, L.F.L. Moro, C.A.O. Nascimento, Characterization of crude petroleum by NIR, J. Pet. Sci. Eng. 51 (2006) 127–137, https://doi.org/10.1016/j.petrol.2005.11.014.

[31] H. Chung, Applications of near-infrared spectroscopy in refineries and important issues to address, Appl. Spectrosc. Rev. 42 (2007) 251–285, https://doi.org/10.1080/05704920701293778.
[32] H. Chung, M.-S. Ku, Comparison of near-infrared, infrared, and Raman spectroscopy for the analysis of heavy petroleum products, Appl. Spectrosc. 54 (2000) 239–245.
[33] C. Pasquini, Near infrared spectroscopy: a mature analytical technique with new perspectives – a review, Anal. Chim. Acta 1026 (2018) 8–36, https://doi.org/10.1016/j.aca.2018.04.004.
[34] P.J. Linstrom, W.G. Mallard (Eds.), NIST Chemistry WebBook, NIST Standard Reference Database Number 69, National Institute of Standards and Technology, Gaithersburg MD, 2018, p. 20899, https://doi.org/10.18434/T4D303.
[35] Q. Wen, J. Shen, Z. Shi, E. Dy, K.H. Michaelian, C. Fairbridge, N.G.C. Astrath, J. H. Rohling, M.L. Baesso, Temperature coefficients of the refractive index for hydrocarbons and binary mixtures, Chem. Phys. Lett. 539–540 (2012) 54–57, https://doi.org/10.1016/j.cplett.2012.05.036.
[36] Q. Wen, J. Shen, R. Gieleciak, K.H. Michaelian, J.H. Rohling, N.G.C. Astrath, M. L. Baesso, Temperature coefficients of the refractive index for complex hydrocarbon mixtures, Int. J. Thermophys. 35 (2014) 930–941, https://doi.org/10.1007/s10765-014-1604-6.
[37] J. Hädrich, The Lorentz-Lorenz function of five gaseous and liquid saturated hydrocarbons, Appl. Phys. 7 (1975) 209–213, https://doi.org/10.1007/BF00936026.
[38] A.Z. Tasic, B.D. Djordjevic, D.K. Grozdanic, N. Radojkovic, Use of mixing rules in predicting refractive indexes and specific refractivities for some binary liquid mixtures, J. Chem. Eng. Data 37 (1992) 310–313, https://doi.org/10.1021/je00007a009.
[39] O.M.D. Lutz, G.K. Bonn, B.M. Rode, C.W. Huck, Reproducible quantification of ethanol in gasoline via a customized mobile near-infrared spectrometer, Anal. Chim. Acta 826 (2014) 61–68, https://doi.org/10.1016/j.aca.2014.04.002.
[40] D.A. Burns, E.W. Ciurczak, E.W. Ciurczak, Handbook of Near-Infrared Analysis, CRC Press, 2007, https://doi.org/10.1201/9781420007374.
[41] Q. Song, F. Huang, M. Li, B. Xie, H. Wang, Y. Jiang, Y. Song, Graded refractive-index SiOx infrared filters prepared by reactive magnetron sputtering, J. Vac. Sci. Technol. A 26 (2008) 265–269, https://doi.org/10.1116/1.2837836.
[42] S.Y. Turishchev, V.A. Terekhov, D.A. Koyuda, A.V. Ershov, A.I. Mashin, E. V. Parinova, D.N. Nesterov, D.A. Grachev, I.A. Karabanova, E.P. Domashevskaya, Formation of silicon nanocrystals in multilayer nanoperiodic a-SiOx/insulator structures from the results of synchrotron investigations, Semiconductors 51 (2017) 349–352, https://doi.org/10.1134/S1063782617030241.
[43] A. García-Valenzuela, R. Alvarez, J.P. Espinós, V. Rico, J. Gil-Rostra, A. Palmero, A. R. Gonzalez-Elipe, SiOx by magnetron sputtered revisited: tailoring the photonic properties of multilayers, Appl. Surf. Sci. 488 (2019) 791–800, https://doi.org/10.1016/j.apsusc.2019.05.273.
[44] J.W. Leem, J.S. Yu, Design and fabrication of amorphous germanium thin film-based single-material distributed Bragg reflectors operating near 2.2 μm for long wavelength applications, JOSA B 30 (2013) 838–842, https://doi.org/10.1364/JOSAB.30.000838.
[45] A. García-Valenzuela, C. López-Santos, V. Rico, R. Alvarez, A. Palmero, A. R. González-Elipe, Environmentally tight TiO2–SiO2 porous 1D-photonic structures, Adv. Mater. Interfaces 6 (2019) 1801212, https://doi.org/10.1002/admi.201801212.
[46] M. Wang, N. Pan, Predictions of effective physical properties of complex multiphase materials, Mater. Sci. Eng. R Rep. 63 (2008) 1–30, https://doi.org/10.1016/j.mser.2008.07.001.
[47] R.L. Scott, P.H. van Konynenburg, Static properties of solutions. Van der Waals and related models for hydrocarbon mixtures, Discuss. Faraday Soc. 49 (1970) 87–97, https://doi.org/10.1039/DF9704900087.

Jorge Gil-Rostra received his Ph. D. degree in 2013 from the University of Sevilla. He is currently researcher at the Institute of Material Science of Seville. His main research interest focus on magnetron sputtering deposition methods, mixed oxides thin films, luminescent materials, optofluidic devices, electrocatalysis and electrochemical sensors.

Sergio Quintero received his M.S. in 2016 from the Polytechnic University of Madrid and is currently obtaining his Ph. D. in the same university. His research interests include the development of optical fiber sensors for chemical, agro-food, and medical applications.

Víctor J. Rico received his Ph. D. in 2010 from the University of Sevilla. Since 2001 he has been a researcher at the Institute of Material Science of Seville. Nowadays, he is working in different areas: metallic electrodes deposited by physical vapour deposition for electrocatalytic studies, development of anti-icing surfaces, and fenestration.

Francisco Yubero received his Ph. D. degree in physics at the Autonomous University of Madrid in 1993. He is Research Scientist from CSIC Spain. His research focuses on theoretical aspects related to surface electron spectroscopies, and the development of photonic sensors based on nanostructured porous thin films.

Francisco J. Sanza received his Ph. D. degree in 2015 from the Polytechnic University of Madrid. He is Invited Researcher at Center for Biomedical Technology belonging to Polytechnic University of Madrid, and also works as Technical Director in Bio Optical Detection S.L. since 2017.

Rafael Casquel received his Ph. D. from the Polytechnic University of Madrid in 2012. Currently he works as Associate Professor at the same university. His research is focused in the field of optical biosensors within the Centre for Biomedical Technology.

Emilio Gallo-Valverde received his degree in Industrial Engineering in 1999 at Carlos III University. He is currently Project Manager at INDRA (Oil&Gas). His work focuses on development and implementation of software to surveillance marine surface to prevent and contain oil splis, Hydrocarbon Early and Automatic Detection System (HEADS).

María E. Jara Galán received her Mining Engineering degree in 1994 at the Polytechnic University of Madrid. Currently she is Head of Portfolio Development at INDRA (Oil&Gas). She is responsible for the development and implementation of a new product portfolio strategy, business development, and commercialisation of new oil&gas products, helping customers in its digital transformation and in the adoption of emerging technologies.

Paula Sanz-Sanz received her Chemical Engineering degree in 2003 from Valladolid University. She is currently Senior Scientist in Production Engineering for E&P at REPSOL Technology Lab. Specialist in fluid-dynamic multiphase flow simulation models and flow assurance assessment of production systems for oil&gas fields.

Miguel Holgado received his Ph. D. degree from the Polytechnic University of Madrid and the Institute of Material Science of Madrid in 2000. He is currently leader of the Optics, Photonics, and Biophotonics Group at Center for Biomedical Technology, and Titular Professor with the Applied Physics and Materials Engineering Department of the Industrial Engineering School at the Polytechnic University of Madrid. He is also the founder of Bio Optical Detection S.L.

Agustín R. González-Elipe received his Ph.D. degree in 1978 from the University Complutense of Madrid. He is currently Research Professor of CSIC at the Institute of Materials Science of Sevilla where he deals with the development of use of nanostructured thin films as photonic and electrochemical sensors.